RSC Advances

A facile approach to construct BiOI/Bi5O7I composites with heterostructure: efficient charge separation and enhanced photocatalytic activity

Journal:	*RSC Advances*
Manuscript ID:	RA-ART-07-2015-013755.R1
Article Type:	Paper
Date Submitted by the Author:	14-Aug-2015
Complete List of Authors:	Yu, Yao-Guang; Harbin Institute of Technology (HIT), Department of chemistry Chen, Gang; Harbin Institute ofTechnology, Department of Chemistry Wang, Xu; Harbin Institute of Technology, Department of chemistry Jia, Dechang; Institute for Advanced Ceramics, Tang, Pengxiao; Harbin Institute of Technology, Department of chemistry Lv, Chade; Harbin Institute of Technology, Department of chemistry; Harbin Institute of Technology, Chemistry

RSC Advances

ARTICLE

A facile approach to construct BiOI/Bi_5O_7I composites with heterostructure: efficient charge separation and enhanced photocatalytic activity

Received 00th January 20xx,
Accepted 00th January 20xx

DOI: 10.1039/x0xx00000x

www.rsc.org/

Yaoguang Yu,[a] Gang Chen,*[a] Xu Wang,[a] Dechang Jia,*[b] Pengxiao Tang,[a] Chade Lv[a]

A series of BiOI/Bi_5O_7I composite photocatalysts with heterostructure was successfully synthetized through a facile hydrothermal method. Attributed to the heterostructure between BiOI and Bi_5O_7I, photogenerated electrons and holes can be separated efficiently. The photocatalytic activity of the as-prepared samples was evaluated through MO degradation reaction. The removal rate of MO was up to 93% after 40 min under visible light ($\lambda \geq 400$ nm) irradiation, while the photocatalytic activity showed no decay after 3 cycles. Furthermore, photocatalytic mechanism of MO degradation over the BiOI/Bi_5O_7I composite photocatalyst was investigated through taking TA, H_2O_2 and EDTA as probes. The experimental results indicate that the enhanced photocatalytic performance is attributed to the synergistic effect of photogenerated holes and superoxide radical. The excellent activity and photostability reveal that the BiOI/Bi_5O_7I composite photocatalyst is a promising visible-light-response photocatalyst with potential application in the field of water treatment.

1. Introduction

Environmental pollution caused by organic pollutants has become a crisis all over the world. However, numerous organic compounds are resistant to the traditional biological and physical removal methods such as adsorption, ultrafiltration and coagulation. Alternative advanced techniques to chemically transform these hazardous compounds into CO_2 and H_2O are urgently required.[1, 2] Among the advanced techniques, semiconductor-based photodegradation process could transform organic pollutants into non-hazardous compounds utilizing solar energy and O_2 as energy source and oxidant, which exhibits highly selective and eco-friendly features.

In recent years, Bi-based semiconductor photocatalysts received much attention due to their broad-band visible light response and outstanding photocatalytic performance for organic compounds degradation. For instance, Yu et al.[3] synthesized monoclinic-phase $BiVO_4$ photocatalyst through a NaF-mediated hydrothermal process. NaF induced surface fluorination of $BiVO_4$ photocatalyst improves the RhB adsorption and accelerates the transfer of photogenerated holes between dye molecule and photocatalyst. Zhu et al.[4] synthesized a series of Bi_2WO_6 photocatalysts through a hydrothermal method by controlling the pH value of the reaction solution. It is found that the crystallinity of Bi_2WO_6 can be tuned by adjusting the pH value of the reaction solution. The improved crystallinity shows positive effect on the photodegradation of Bisphenol A. Moreover, Nan et al.[5] synthesized the microsphere-like BiOI photocatalyst through a one-step solution method at room temperature. The as-prepared BiOI photocatalyst with hierarchical structure exhibits mesoporous surface layer, which shows outstanding capacity for the photodegradation of tetracycline hydrochloride. In addition, Bi_5O_7I, which has a similar layer structure with BiOI, was firstly reported by Wang and co-workers for photodegradation of RhB in water and acetaldehyde in air under visible light irradiation.[6] The relative more positive valence band potential of Bi_5O_7I compared with other bismuth oxyiodides would provide more active holes to oxidize the organic pollutants. According to the previous literature, construction of composite photocatalysts with heterostructure is a promising strategy to improve photocatalytic activity, which would exhibit superior performance compared with their single component photocatalysts.[7] Accordingly, BiOCl/BiOI,[8] Bi_5O_7I/Bi_2O_3[9] and BiO_pBr_q/BiO_mI_n[10] composite photocatalysts with heterostructure are synthetized showing outstanding performance for the degradation of organic pollutants. However, the report on the BiOI/Bi_5O_7I composite photocatalyst is still rare.

In this work, a series of BiOI/Bi_5O_7I composite photocatalysts with heterostructure was successfully

[a] Department of Chemistry, Harbin Institute of Technology, Harbin 150001, P. R. China, E-mail: gchen@hit.edu.cn, ygyu@hit.edu.cn, Tel: +86-451-86403117.
[b] Institute for Advanced Ceramics, School of Materials Science and Engineering, Harbin Institute of Technology, Harbin 150001, P. R. China, E-mail: dcjia@hit.edu.cn

synthesized through hydrothermal method by adjusting the pH value. MO was used as the target dye to evaluate the photocatalytic performance of the composite photocatalyst. Moreover, TA, H_2O_2 and EDTA were introduced as probes to investigate the intermediate active oxidants. Finaly, a photocatalytic mechanism was proposed based on the experimental results to provide an insight into the reaction process over the composite photocatalyst with heterostructure.

2. Experiemtal

2.1 Synthesis of BiOI and BiOI/Bi_5O_7I composites

BiOI and BiOI/Bi_5O_7I composites were synthesized through the hydrothermal method. All the chemicals were of analytical grade and used without further purification. In a typical synthesis procedure, 0.485 g $Bi(NO_3)_3$•$5H_2O$ was added into 17 mL absolute ethanol under continuous stirring at room temperature for 30 min. The aforementioned solution was then added dropwise into 17 mL KI solution (0.166 g KI dissolved in 17 mL distilled water). NH_3•H_2O was used to adjust the pH value (pH=7, 9 and 11). After additional stirring for 20 min, the mixture was transferred into a 50 mL Teflon-lined stainless steel autoclave, which was sealed and maintained at 140 ^oC for 24 h. Subsequently, the autoclave was naturally cooled to room temperature. Then, the products were collected and washed sequentially with distilled water and ethanol. Finally, the collection was dried at 60 ^oC for 8 h.

2.2 Characterization

X-ray diffraction (XRD) patterns of the samples were obtained on a Rigaku D/max-2000 diffractometer, with monochromated Cu Kα radiation (45 kV, 50 mA). The morphology of as-prepared samples was characterized by field-emission scanning electron microscopy (FESEM, FEI Quanta 200F) and transmission electron microscopy (TEM, Tecnai G^2 S-Twin). Brunauer-Emmett-Teller (BET) specific surface area was measured through Builder 4200 instrument at liquid nitrogen temperature (195.8 ^oC). UV-vis diffuse reflectance spectra were acquired by a spectrophotometer (TU-1900). The UV-vis absorption spectra were converted from UV-vis diffuse reflectance spectra through the standard Kubelka-Munk method. $BaSO_4$ was used as the reflectance standard. The photoluminescence (PL) spectra were measured at room temperature with a fluorescence spectrophotometer (Perkin Elmer LS55). The excitation wavelength of the as-prepared samples and terephthalic acid (TA) was 260 and 320 nm, respectively.

2.3 Mott-Schottky measurement

The flat band potentials (E_{fb}) of BiOI and Bi_5O_7I were determined by Mott–Schottky method, which was carried out in a conventional three electrode cell using an Autolab PGSTAT 302N potentiostat/galvanostat. The as-prepared sample was deposited as a film on a 1 cm × 1 cm area of a 1 cm × 2 cm FTO glass as the photoanode, and the ohmic contact between the photoanode and the copper conductor was made on the non-photocatalyst coated part of FTO glass using conductive adhesives. An Ag/AgCl electrode was used as the reference electrode, and Pt was used as the counter electrode. The electrolyte was 0.5 mol•L^{-1} Na_2SO_4 aqueous solution.

2.4 Photocatalytic test

The photocatalytic performance of the samples was evaluated from the photodegradation of methyl orange (MO) under irradiation with visible light (a 300W Xe lamp with a 400 nm cut-off filter). In each experiment, sample powder (0.05g) was suspended evenly in 100 mL of 10.0 mg•L^{-1} MO aqueous solution in a quartz reactor. Before illumination, the suspensions were constantly stirred for 40 min in the dark to establish an adsorption-desorption equilibrium. The concentration of MO during the catalytic reaction was measured by detecting the change of the maximum absorbance peak at 464 nm.

3. Results and discussion

3.1 Crystal structure and morphology

The XRD patterns of the samples synthesized at different pH values are shown in Fig. 1. The XRD pattern of Bi_5O_7I photocatalyst, which is synthesized according to Wang's method,[6] is also recorded for comparison. It is found that all the diffraction peaks of the sample prepared at pH=7 are in good agreement with the tetragonal BiOI phase (JCPDS No. 10-0445). No other diffraction peaks corresponding to impurity phase are detected. With the increase of pH value, orthorhombic Bi_5O_7I phase (JCPDS No. 40-0548) appeared. It can be seen that diffraction peaks corresponding to orthorhombic Bi_5O_7I phase are detected in the sample synthesized at pH=9, which indicates the coexistence of BiOI and Bi_5O_7I. When the pH value is further adjusted to 11, diffraction peaks corresponding to orthorhombic Bi_5O_7I become dominant. The composition of BiOI/Bi_5O_7I composites synthetized at different pH values (pH=9, 11) can be obtained based on the EDS results (Table S1). It can be seen that the amount of BiOI in the BiOI/Bi_5O_7I composites decreases with the increase of the pH value (from 0.64 at pH=9 to 0.2 at pH=11). The detailed reaction mechanism is discussed as following.

When the KI aqueous solution was added to the $Bi(NO_3)_3$ ethanol solution, $Bi(NO_3)_3$ would firstly be hydrolyzed to slightly soluble $BiONO_3$ as shown in Reaction 1, which have been previously reported.[11, 12]

$$Bi(NO_3)_3+H_2O \longrightarrow BiONO_3+2NO_3^-+2H^+ \quad (1)$$

Due to the fast reaction rate between $BiONO_3$ and I^- (Reaction 2), the red BiOI appeared immediately after mixing the abovementioned solutions.

$$BiONO_3+I^- \longrightarrow BiOI+NO_3^-$$

(2)

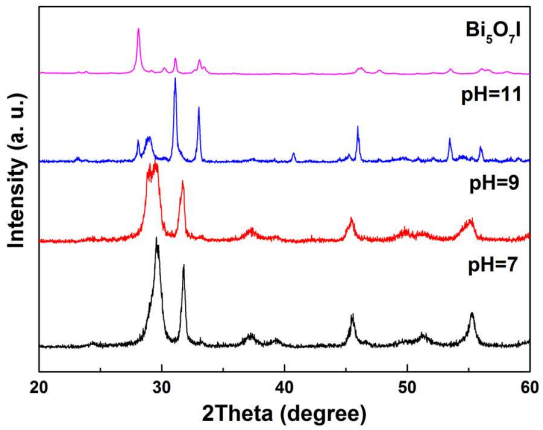

Fig. 1 XRD patterns of samples synthesized at different pH values (pH=7, 9, 11) and pure Bi_5O_7I.

When the $NH_3 \bullet H_2O$ was added to the reaction system, Bi_5O_7I will be produced according to Reaction 3. Further increasing the pH value would force the equilibrium of Reaction 3 to shift toward the positive direction due to the increasing amount of OH^-.

$$5BiONO_3+I^-+4NH_3 \cdot H_2O \longrightarrow Bi_5O_7I+2H_2O+4NH_4^++5NO_3^-$$

(3)

It is obvious that Reaction 2 and Reaction 3 are competing reactions. Properly controlling the pH value of the reaction solution would make the composition of the composite adjustable, which indicates pH value is a crucial factor for synthetizing BiOI/Bi_5O_7I composite. Therefore, the relatively high pH value would be beneficial to the formation of iodine-poor bismuth oxyiodide, which is consistent with the previous report.[13]

In order to investigate the effect of morphology on the photocatalytic performance, the morphology feature of BiOI/Bi_5O_7I composite synthesized at pH=9 with the highest performance among the tested samples was characterized by FESEM and TEM. The FESEM image (Fig. 2a) clearly reveals that the obtained BiOI/Bi_5O_7I composite synthesized at pH=9 is composed of flower-like microspheres with an average diameter of *ca*. 1–2 μm. The inset in Fig. 2a, which presents the high-magnification FESEM image of the BiOI/Bi_5O_7I composite synthesized at pH=9, shows that the flower-like microsphere is composed of nanoflakes with a thickness of *ca*. 35-40 nm. The morphology of BiOI, BiOI/Bi_5O_7I composite synthesized at pH=11 and Bi_5O_7I is shown in Fig S1 for comparison. The TEM image (Fig. 2b) further exhibits that the nanoflakes aggregate in a random array. They connect to each other tightly through the dark center of the flowers. In order to explore the detailed crystal structure of the nanoflakes, a petal of an individual microsphere is closely investigated through HRTEM (Fig. 2c). It can be seen from Fig. 2d that the lattice spacing of 0.317 nm corresponds to the (312) plane of orthorhombic Bi_5O_7I phase. The corresponding FFT pattern (Fig. 2e) further confirms the single crystal nature of the selected region. In contrast, the lattice spacing of 0.282 nm in Fig. 2f can be indexed as the (110) plane of tetragonal BiOI phase. Moreover, it can be seen that the FFT pattern can be indexed to the [001] zone axis of the tetragonal matlockite structure, which is completely different from the FFT pattern transformed from Fig. 2d. This evidence confirms the existence of two phases in one nanoflake and further indicates the formation of tight heterojunction between BiOI and Bi_5O_7I in nano level. Moreover, the heterostructure between BiOI and Bi_5O_7I will be beneficial to the separation of photogenerated carriers and thus improve the photocatalytic performance.

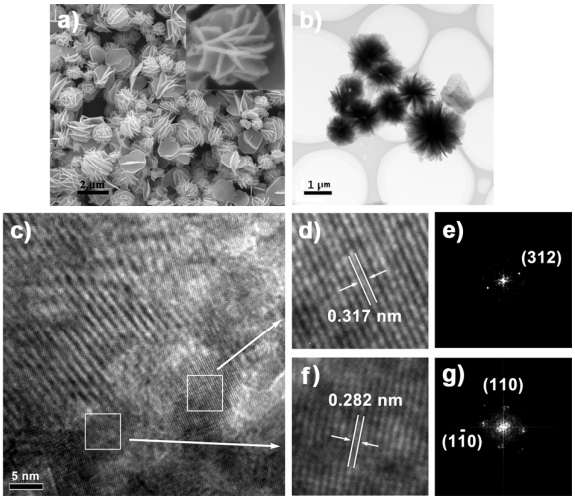

Fig. 2 Morphology observation of BiOI/Bi_5O_7I composite synthesized at pH=9: a) low-magnification FESEM image of the overall morphology; b) low-magnification TEM image of the flower-like microspheres; c) HRTEM image of the nanoflake; d) enlarged HRTEM image of orthorhombic Bi_5O_7I phase; e) the corresponding FFT pattern; f) enlarged HRTEM image of tetragonal BiOI phase and g) the corresponding FFT pattern. The inset in a) is the enlarged view of an individual microsphere. The side length of d) and e) is 5 nm.

3.2 Optical absorption properties and energy band positions

The optical absorption property of the samples synthesized at different pH values (pH=7, 9, 11) and pure Bi_5O_7I was investigated by UV-vis absorption spectroscopy (Fig. 3a). With the increase of pH value, the absorption edge of samples synthesized at different pH values monotonously shifts towards the short-wavelength direction. All the BiOI/Bi_5O_7I composites have intense absorptions in the visible light region. The absorption edge of BiOI/Bi_5O_7I composite synthesized at pH=9 is at *ca*. 550 nm, which reveals a good visible light response. In contrast, the orthorhombic Bi_5O_7I can only absorb

part of visible light. The optical band gap energy of a crystalline semiconductor could be calculated by the following formula[14]:

$$\alpha h\nu = A(h\nu - E_g)^{n/2} \quad (4)$$

where α, h, ν, A and E_g are the absorption coefficient, Planck constant, light frequency, proportionality constant and band gap, respectively. In the equation, n depends on the characteristics of the transition in a semiconductor, for instance, n=1 for a direct transition semiconductor, whereas n=4 for an indirect transition semiconductor. From the linear relationship between $(\alpha h\nu)^{1/2}$ and photon energy, the band energy (E_g) could be obtained by the intercept of the tangent to the linear region of the plot with abscissa. According to the literature,[6, 15] the value of n for Bi_5O_7I is estimated to be 2, whereas n for BiOI is estimated to be 4. Following this method, the band gaps of pure BiOI and Bi_5O_7I are determined to be 1.90 eV and 2.90 eV, respectively.

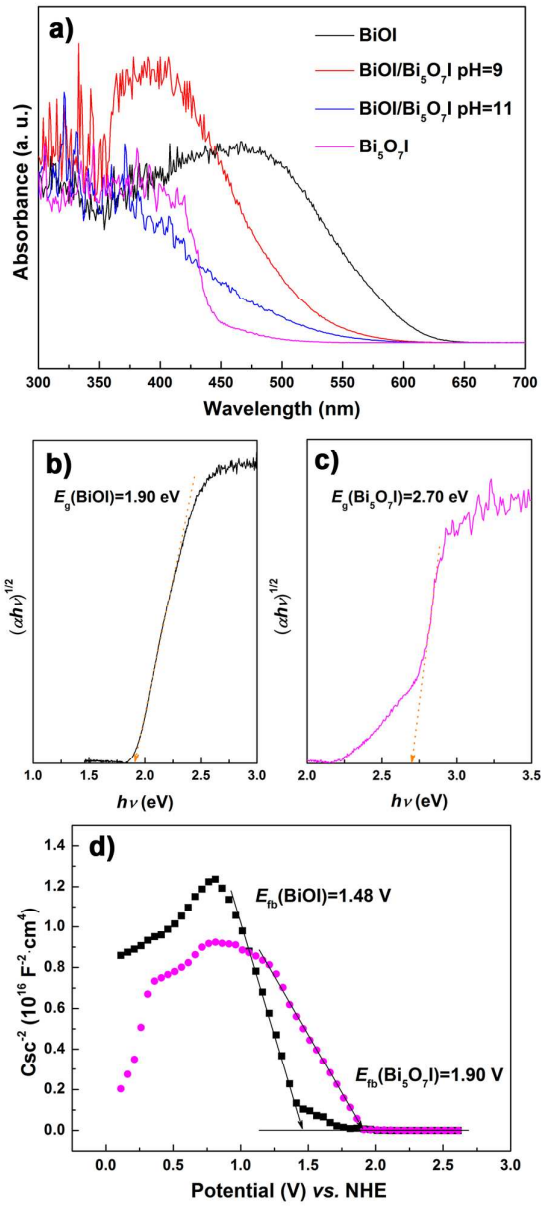

Fig. 3 a) UV-vis absorption spectra of samples synthesized at different pH values (pH=7, 9, 11) and pure Bi_5O_7I; tauc plots of b) pure BiOI and c) Bi_5O_7I; d) Mott–Schottky plots for BiOI and Bi_5O_7I.

The energy band positions can be obtained through the band gap values combined with either conduction or valence band position. Mott-Schottky method is an effective way to determine the flat band position of semiconductors (approximately equals to the conduction band minimum for n-type semiconductor and the valence band maximum for p-type semiconductor).[16, 17] Accordingly, the flat band positions of BiOI and Bi_5O_7I is obtained as shown in Fig 3d. The negative slopes of Mott–Schottky plots indicate both BiOI and Bi_5O_7I are p-type semiconductors, which means the valence band

maximum of BiOI and Bi_5O_7I are 1.48 V and 1.90 V (*vs*. NHE), respectively. Therefore, valence band positions and conduction band positions of BiOI and Bi_5O_7I can be obtained (Scheme 1).

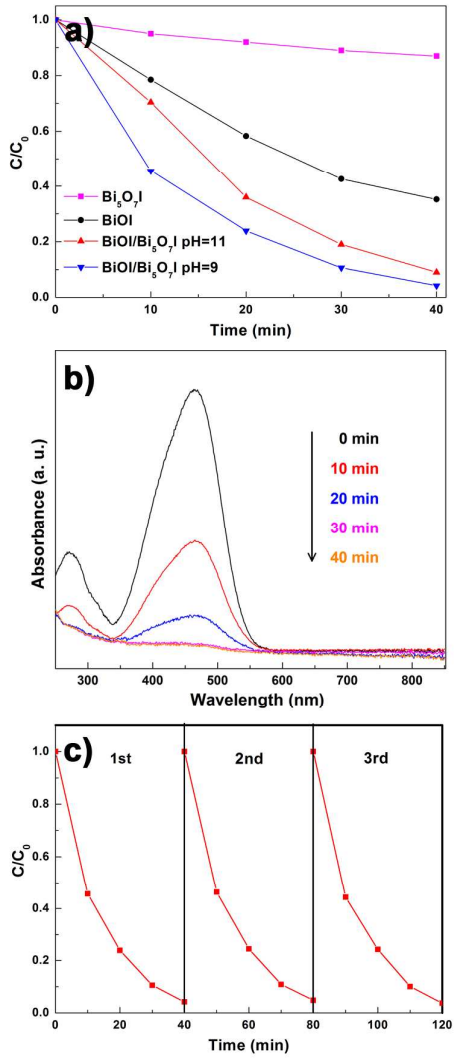

Fig. 4 a) Photodegradation of MO as a function of irradiation time over samples synthesized at different pH values (pH=7, 9, 11) and pure Bi_5O_7I; b) UV-vis spectra and c) cycling runs of MO as a function of irradiation time over BiOI/Bi_5O_7I composite synthesized at pH=9.

3.3 Photocatalytic performance and mechanism

Methyl Orange (MO), which shows a major absorption band at 464 nm, is selected as a representative model pollutant to evaluate the photocatalytic performance of pure BiOI, Bi_5O_7I and BiOI/Bi_5O_7I composites under visible light irradiation ($\lambda \geqslant$ 400 nm). Fig. 4a illustrates temporal evolution of the concentration change during the MO photodegradation process over samples synthesized at different pH values (pH=7, 9, 11) and pure Bi_5O_7I. The BiOI/Bi_5O_7I composite synthesized at pH=9 exhibits the highest photocatalytic performance among all the tested samples, and the removal rate of MO is up to 93% after 40 min visible light irradiation. In contrast, the removal rate of MO by using pure BiOI and Bi_5O_7I is 64% and 13%, respectively. It should be noted that the specific surface areas of BiOI, BiOI/Bi_5O_7I composite synthesized at pH=9, 11 and Bi_5O_7I are 7.1, 5.9, 5.8 and 3.0 $m^2 \bullet g^{-1}$, respectively. This means the enhanced performance of BiOI/Bi_5O_7I composite is not due to the increase of specific surface area. Fig. 4b shows the UV-vis spectra of MO aqueous solution in the presence of BiOI/Bi_5O_7I composite synthesized at pH=9 under different irradiation time. During the photocatalytic reaction, no new absorption band is detected in either UV or visible region, which demonstrates the complete elimination of chromogenic functional groups in MO (destruction of azo bonds).[18] Moreover, the stability of BiOI/Bi_5O_7I composite synthesized at pH=9 is tested through recycling experiments (Fig. 4c). It can be seen that MO can be decomposed within 40 min in all the three cycles, which indicates the BiOI/Bi_5O_7I composite photocatalyst is stable during photocatalytic process and thus a promising photocatalyst for practical application in water treatment.

Photoluminescence (PL) spectroscopy was introduced to analyze the charge separation of the as-prepared photocatalysts (Fig. 5a). When the excitation wavelength of the incident light is set to be 260 nm, PL emission from all the specimens could be observed at around 400 nm. However, the intensity of these peaks decreases in a sequence of Bi_5O_7I > BiOI > BiOI/Bi_5O_7I (pH=9). This phenomenon exhibits that the recombination of photogenerated electrons and holes is greatly depressed, which demonstrates the efficient separation of photogenerated carriers within the heterostructure between BiOI and Bi_5O_7I. In order to investigate the probable photocatalytic mechanism, the terephthalic acid (TA) was introduced as the probe molecule to monitor the formation of hydroxyl radicals (•OH) through a photoluminescence method.[19] When •OH is captured by the nonfluorescent terephthalic acid, the highly fluorescent 2-hydroxyterephthalic acid with an emission wavelength at 420 nm upon excitation wavelength of 320 nm would be produced.[20] As a result, the amount of •OH produced by the photocatalyst can be monitored by the change of the fluorescence intensity. It can be seen from Fig. 5b that the fluorescent signal from all the specimens are almost undetectable and changed nonlinearly with the irradiation time, which means almost no •OH is formed in the suspension during the illumination process. The aforementioned result suggests •OH is not the active intermediate in the process of MO degradation over the BiOI/Bi_5O_7I (pH=9) composite photocatalyst.

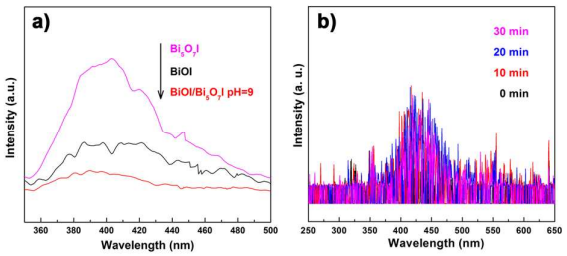

Fig. 5 a) Photoluminescence spectra of pure BiOI, Bi_5O_7I and $BiOI/Bi_5O_7I$ composite synthesized at pH=9; b) time-dependent photoluminescence spectra of $BiOI/Bi_5O_7I$ composite synthesized at pH=9 in 0.4 mmol•L^{-1} terephthalic acid solution. The reaction solution was irradiated with visible light ($\lambda \geq$ 400 nm) and sampled every 10 min.

Towards a better understanding of the photodegradation mechanism over the $BiOI/Bi_5O_7I$ composite photocatalyst, H_2O_2 and ethylenediaminetetraacetic acid (EDTA) were added to the reaction solution as electron acceptor and hole scavenger, respectively.[21, 22] It can be seen from Fig. 6a that the photocatalytic performance of the $BiOI/Bi_5O_7I$ (pH=9) composite photocatalyst decreases remarkably in the presence of either H_2O_2 or EDTA, which demonstrates both electrons and hole are essential to the photodegradation of MO. According to the literature, photogenerated electrons could react with O_2 to produce superoxide radical ($O_2^{-\bullet}$).[23] The consumption of photogenerated electrons by adding H_2O_2 would directly inhibit the formation of $O_2^{-\bullet}$. In order to further explore the possible sensitized effect of the dye on the photocatalytic reaction over the as-prepared composite photocatalysts, the photocatalytic performance of the the $BiOI/Bi_5O_7I$ (pH=9) composite photocatalyst from the photodegradation of MO under 350 and 475 nm incident monochromatic light is evaluated, respectively. Because the MO aqueous solution shows almost no absorption when the wavelength of the incident monochromatic light is 350 nm. A 350 nm band pass is used to test the contribution of MO degradation from composite photocatalyst. In contrast, due to the maximum absorbance peak of MO is at 464 nm, a 475 nm band pass is used to test the contribution of MO degradation from dye sensitized effect. It can be seen from Fig. 6b that the photocatalytic performance is similar under 350 and 475 nm monochromatic light irradiation, which means both electrons from the MO molecules and carriers from the composite photocatalyst contribute to the degradation of MO. Therefore, the enhanced photocatalytic performance of MO degradation over the $BiOI/Bi_5O_7I$ (pH=9) composite photocatalyst can be attributed to the synergistic effect of photogenerated holes and superoxide radical.

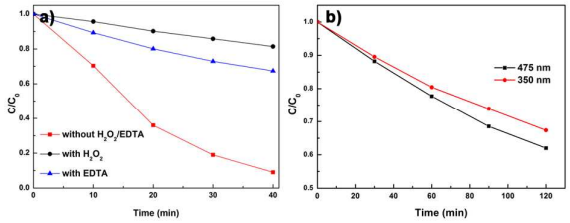

Fig. 6 Photodegradation of MO a) in the presence of H_2O_2 (1.5 mL 35% H_2O_2 per 100 mL MO solution) or EDTA (10^{-3} mol•L^{-1}) and b) under 350 and 475 nm incident monochromatic light irradiation.

Based on the aforementioned experimental results, a scheme is proposed to discuss the photocatalytic mechanism of MO degradation over the $BiOI/Bi_5O_7I$ composite photocatalyst (Scheme 1). When $BiOI/Bi_5O_7I$ composite photocatalyst is exposed to the visible light irradiation, electrons in the valence bands of both BiOI and Bi_5O_7I would be excited to the conduction bands. Under visible light irradiation ($\lambda \geq$ 400 nm), the maximum energy of a single photon is 3.1 eV. In the case of BiOI, the valence electrons (potential of valence band is 1.48 V *vs*. NHE) would be excited to a higher level after reaching the inherent conduction band with the irradiation of incident visible light.[8, 24] The potential of the newly reached conduction band (-1.62 V) is negative enough to trigger the one-electron reduction of O_2 to $O_2^{-\bullet}$ (-0.16 V).[25] Similarly, Bi_5O_7I with a newly reached conduction band (-1.20 V) could also reduce O_2 to $O_2^{-\bullet}$ under visible light irradiation. In such a composite system, photogenerated electrons in the newly reached conduction band of BiOI can transfer to the newly reached conduction band of Bi_5O_7I. In the meanwhile, photogenerated holes in the valence band of Bi_5O_7I can ransfer to the valence band of BiOI. As a consequence, photogenerated electrons and holes could be effectively separated by the heterostructure between BiOI and Bi_5O_7I.

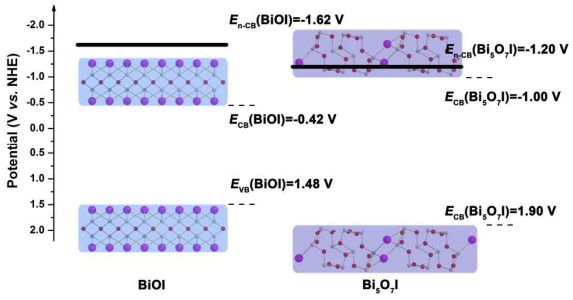

Scheme 1 The proposed possible mechanism for the enhanced photocatalytic performance.

4. Conclusion

In summary, a series of $BiOI/Bi_5O_7I$ composite photocatalysts with heterostructure was successfully synthesized through

hydrothermal method by adjusting the pH value. The as-prepared composite photocatalysts exhibited enhanced photocatalytic performance for MO degradation compared with the single-phase photocatalysts. The heterostructure between BiOI and Bi_5O_7I was believed to play a key in separating photogenerated carriers. The photocatalytic mechanism of MO degradation over the BiOI/Bi_5O_7I composite photocatalyst is confirmed to be the synergistic effect of photogenerated holes and superoxide radical. Under such a synergistic effect, the removal rate of MO was up to 93% after 40 min visible light ($\lambda \geq$ 400 nm) irradiation. Moreover, the BiOI/Bi_5O_7I composite photocatalyst showed good durability, which is a potential candidate for environmental applications.

Acknowledgement

This work was financially supported by projects of Natural Science Foundation of China (21271055, 21471040), China Postdoctoral Science Foundation (2015M571409), Fundamental Research Funds for the Central Universities and Program for Innovation Research of Science in Harbin Institute of Technology (PIRS OF HIT Q201507).

Notes and references

1. A. B. Djurišić, Y. H. Leung and A. M. Ching Ng, *Mater. Horiz.*, 2014, **1**, 400-410.
2. K. Rajeshwar, A. Thomas and C. Janáky, *J. Phys. Chem. Lett.*, 2015, **6**, 139-147.
3. S. Liu, K. Yin, W. Ren, B. Cheng and J. Yu, *J. Mater. Chem.*, 2012, **22**, 17759-17767.
4. C. Wang, H. Zhang, F. Li and L. Zhu, *Environ. Sci. Technol.*, 2010, **44**, 6843-6848.
5. R. Hao, X. Xiao, X. Zuo, J. Nan and W. Zhang, *J. Hazard. Mater.*, 2012, **209-210**, 137-145.
6. S. M. Sun, W. Z. Wang, L. Zhang, L. Zhou, W. Z. Yin and M. Shang, *Environ. Sci. Technol.*, 2009, **43**, 2005-2010.
7. H. Li, Y. Zhou, W. Tu, J. Ye and Z. Zou, *Adv. Funct. Mater.*, 2015, **25**, 998-1013.
8. T. B. Li, G. Chen, C. Zhou, Z. Y. Shen, R. C. Jin and J. X. Sun, *Dalton Trans.*, 2011, **40**, 6751-6758.
9. L. Cheng, X. Liu and Y. Kang, *Mater. Lett.*, 2014, **134**, 218-221.
10. Y. R. Jiang, S. Y. Chou, J. L. Chang, S. T. Huang, H. P. Lin and C. C. Chen, *RSC Adv.*, 2015, **5**, 30851-30860.
11. C. Liu and D. Zhang, *Chem. Eur. J.*, 2015, DOI: 10.1002/chem.201500383.
12. J. Liu, H. Li, N. Du, S. Song and W. Hou, *RSC Adv.*, 2014, **4**, 31393-31399.
13. X. Xiao and W. D. Zhang, *RSC Adv.*, 2011, **1**, 1099- 1105.
14. Y. Lei, G. Wang, S. Song, W. Fan, M. Pang, J. Tang and H. Zhang, *Dalton Trans.*, 2010, **39**, 3273-3278.
15. X. Xiao and W. D. Zhang, *J. Mater. Chem.*, 2010, **20**, 5866-5870.
16. S. J. Hong, S. Lee, J. S. Jang and J. S. Lee, *Energy Environ. Sci.*, 2011, **4,** 1781-1787.
17. T. W. Kim and K. S. Choi, *Science*, 2014, **343,** 990-994.
18. J. Zhang, F. Shi, J. Lin, D. Chen, J. Gao, Z. Huang, X. Ding and C. Tang, *Chem. Mater.*, 2008, **20**, 2937-2941.
19. C. Li, F. Wang, J. Zhu and J. C. Yu, *Appl. Catal. B-Environ.*, 2010, **100**, 433-439.
20. V. Rajendran, M. Lehnig and C. M. Niemeyer, J. Mater. Chem., 2009, 19, 6348-6353.
21. J. Zhou, C. Deng, S. Si, Y. Shi and X. Zhao, *Electrochim. Acta*, 2011, **56**, 2062-2067.
22. J. Fernández, J. Kiwi, J. Baeza, J. Freer, C. Lizama and H. D. Mansilla, *Appl. Catal. B-Environ.*, 2004, **48**, 205-211.
23. L. Zhang, F. Sun, Y. Zuo, C. Fan, S. Xu, S. Yang and F. Gu, *Appl. Catal. B-Environ.*, 2014, **156-157**, 293-300.
24. Y. Li, J. Wang, H. Yao, L. Dang and Z. Li, *Catal. Commun.*, 2011, **12**, 660-664.
25. C. Chen, W. Ma and J. Zhao, *Chem. Soc. Rev.*, 2010, **39**, 4206-4219.

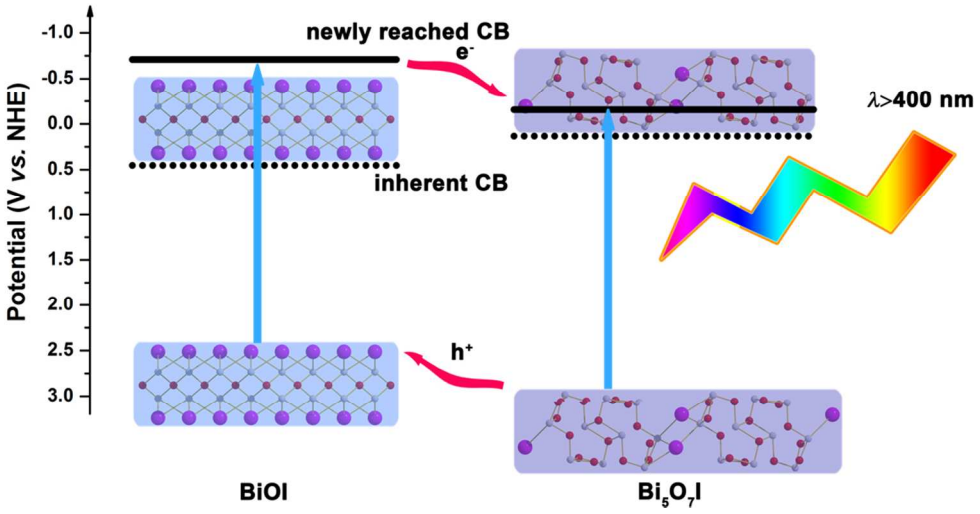

99x51mm (300 x 300 DPI)